# Supporting Information for

# Photoinduced Sign Change of Magnetoresistance in Field-Effect Transistors based on a Bipolar Molecular Glass

***Evgeny Tatarov,[‡a] Thomas Reichert,[‡a] Tobat P. I. Saragi,*[a] Ayna Scheffler,[a] Roman Ueberschaer,[a] Clemens Bruhn,[b] Thomas Fuhrmann-Lieker[a] and Josef Salbeck[a]***

[a] *Macromolecular Chemistry and Molecular Materials, Institute of Chemistry, Department of Mathematics and Science and Center for Interdisciplinary Nanostructure Science and Technology (CINSaT), University of Kassel, D 34132 Kassel, Germany.*
*Tel: +49 561 8044720; E-mail: tobat.saragi@uni-kassel.de*

[b] *Institute of Chemistry, Department of Mathematics and Science, University of Kassel, D 34132 Kassel, Germany.*

CCDC 919918 - 919920 contain the supplementary crystallographic data for this paper. These data can be obtained free of charge from The Cambridge Crystallographic Data Centre via www.ccdc.cam.ac.uk/data_request/cif.

‡These authors contributed equally.

## CONTENT:

**A. Synthesis and characterization of Spiro-DPPFPy**

**B. Preparation and characterization of OFETs**

**C. Output and transfer curves of Spiro-DPPFPy OFETs**

**D. Output and transfer curves of Spiro-PFPy OFETs**

**E. Data acquisition process and statistics**

**F. Magnetoresistance of illuminated devices**

**G. Magnetic Field Dependence**

## A. Synthesis and characterization of Spiro-DPPFPy

**General.** NMR-spectra were measured with a 500-VNMRS Varian Spectrometer with a ONE-NMR-Probe. The measuring frequencies were 500 MHz ($^{1}$H NMR), 125.7 MHz ($^{13}$C NMR), 470.2 MHz ($^{19}$F-NMR). $^{13}$C NMR data were collected by proton decoupling methods. Chemical shifts (δ) are expressed in ppm and are referenced to the shift of the residual proton impurities of the solvents used relative to trimethylsilane for $^{1}$H and to the solvent signal for $^{13}$C. $^{19}$F NMR samples in $CDCl_3$ are directly referenced to trichlorofluoromethane.

Mass spectra were recorded on a quadrupole ion-trap spectrometer (ESI and APCI) Finnigan LCQ DECA (ThermoQuest, San Jose, USA). HR-ESI Mass spectra were recorded on a micrOTOF spectrometer (Bruker Daltonics, Bremen, Germany). MALDI Mass spectra were recorded on a BiFlex IV (Bruker Daltonics, Bremen, Germany) spectrometer equipped with an $N_2$-Laser with a wavelength of 337 nm and 3 ns pulse duration. DCTB (2-[(2E)-3-(4-*tert*-butylphenyl)-2-methylprop-2-enyliden]-malononitril) was used as matrix. Mass calibration was performed immediately prior to the measurements using polystyrene standard (Ag-Adduct).

The melting point of samples was determined in an instrument of model Diamond TG/TA (Perkin Elmer) with the Pyris-Thermal Analysis software. A heating rate was adjusted at 5 °C/min and $N_2$ flow rate of 200 mL/min. The samples for the DSC analysis were prepared in capsules and subjected to an instrument of model Perkin-Elmer DSC 7X Thermal Analysis System with the Pyris-Thermal Analysis software. The heating rate was 10 °C / min. The melting points are expressed as the peak onset value. The glass transition point values are determined from the second and third heating cycles.

Samples for UV/Vis-spectra were prepared as dilute solutions in 1 cm standard quartz cuvette (Hellma). Dichloromethane (UVASOL 99.9 %, Merck) was used for the sample preparation. UV/Vis-spectra were taken in an instrument of model Lambda 900 UV/Vis/NIR-spectrometer of Perkin-Elmer.

For the reaction monitoring thin-layer chromatography (TLC) was performed on aluminium sheets of Machery-Nagel Alugram SIL G/$UV_{254}$ (40 × 80 mm) pre-coated with silica gel (0.2 mm layer) including fluorescent indicator. The substances were visualized by quenching of ultraviolet fluorescence (λ = 254-366 nm). For the purification of the reaction products, column chromatography was performed under ambient pressure using silica gel (0.064-0.200 mm) of Merck.

**Materials.** 2,7-dibromo-9,9'-spirobifluorene **1** was synthesised according literature procedure [S1]. Toluene was dried over sodium and distilled prior to use. Acetonitrile was dried by distillation over calcium hydride. The 0.024 g/mL solution of *tert*-butyl phosphine in dried toluene was prepared before use and stored under nitrogen atmosphere. All other solvents and reagents were obtained from commercial suppliers and were used without further purification.

**Synthesis of 2,7-Bis-(2,3,5,6-tetrafluoropyridin-4-yl)-9,9'-spirobifluorene (2).** A Young flask was charged with $K_2CO_3$ (0.965 g, 7.00 mmol), $Pd(OAc)_2$ (0.071 g, 0.32 mmol), 2,7-dibromo-9,9'-spirobifluorene **1** (1.500 g, 3.16 mmol). The reaction vessel was evacuated and backfilled with nitrogen three times. 10 mL DMA was then added and the mixture was degassed twice. 1.0 mL of 2,3,5,6-tetrafluoropyridine (9.50 mmol) and 5.2 mL of a P(*tert*-Bu)$_3$ / toluene solution (0.024 g/mL solution, 0.62 mmol) were added via syringe and the reaction was stirred at 110º C for 22 hours. The reaction mixture was cooled to room temperature, concentrated to a volume of approximately 5 mL and then column chromatographed (cyclohexane-DCM 4:1) to yield **2** as a white solid **(**0.867 g, 1.41 mmol, 45 %). Crystals suitable for X-ray measurements were obtained by slow diffusion of *n*-hexane into solution of **2** in $CHCl_3$. Melting point: 258 °C (onset); glass transition temperature: 102 °C; $^1$H NMR ($CDCl_3$): δ 8.05 (d, 2H, $^3J$ = 7.8 Hz), 7.83 (d, 2H, $^3J$ = 7.8 Hz), 7.58 (d, 2H, $^3J$ = 7.8 Hz), 7.39 (t, 2H, $^3J$ = 7.3 Hz), 7.13 (t, 2H, $^3J$ = 7.3 Hz), 6.90 (m, 2H), 6.77 (d, 2H, $J$ = 7.8

Hz); $^{13}$C NMR ($CDCl_3$): δ 150.2, 146.8, 143.9 (m, $^1J_F$ = 246 Hz), 142.7, 141.8, 139.0 (m, $^1J_F$ = 259 Hz), 133.0 (m), 129.8, 128.4, 128.2, 126.1, 125.7, 123.9, 121.1, 120.4, 65.0; $^{19}$F NMR ($CDCl_3$): δ −91.3 (m, 4F), −145.3 (m, 4F); MS (MALDI): *m/z* 614.34 (100, $M^+$); HR-MS (MALDI): calcd for $M^+$, 614.1023; found 614.1038.

**Synthesis of 2,7-Bis-(2,3,5,6-tetrafluoropyridin-4-yl)-2',7'-dibromo-9,9'-spirobifluorene (3).** 0.500 g (0.81 mmol) 2,7-bis(2,3,5,6-tetrafluoropyridin-4-yl)-9,9'-spirobifluorene **2** and 10 mL DCM were placed in a Young flask. 1.55 g (9.72 mmol) of bromine was added drop wise to the reaction solution at 0 °C. The Young flask was closed and the resulting reaction mixture was stirred at 40º C for 65 h. The mixture was poured into saturated aqueous sodium hydrogen sulfite solution (30 mL) and extracted with DCM (2×30 mL). The organic layer was washed with saturated $NaHCO_3$ (30 mL), and finally with water (30 mL). The combined organic phase was dried over magnesium sulfate, filtrated and then dried in vacuum. The isolated compound **3** (0.588 g, 0.76 mmol, 94 %) as a white solid was used for the next reaction without further purification. The X-ray suitable crystals were obtained by slow diffusion of *n*-hexane into solution of **3** in $CHCl_3$. Melting point**:** 246 °C (onset). $^1$H NMR ($CDCl_3$): δ 8.07 (m, 2H, $^3J$ = 8.0 Hz), 7.67 (d, 2H, $^3J$ = 8.2 Hz), 7.64 (d, 2H, $^3J$ = 8.0 Hz), 7.52 (dd, 2H, $^3J$ = 8.2 Hz, $^4J$ = 1.7 Hz), 6.90 (m, 2H), 6.88 (s, 2H); $^{13}$C NMR ($CDCl_3$): δ 148.6, 148.5, 144.0 (m, $^1J_F$ = 246 Hz), 142.6, 139.7, 139.0 (m, $^1J_F$ = 259 Hz), 132.7 (m), 131.9, 130.5, 127.2, 126.5, 125.7, 122.2, 121.8, 121.4, 65.6; $^{19}$F NMR ($CDCl_3$): δ −91.0 (m, 4F), −145.0 (m, 4F); MS (MALDI): *m/z* 771.98 (100%, $M^+$).

**Synthesis of 2,7-Bis-(2,3,5,6-tetrafluoropyridin-4-yl)-2',7'-bis-(*N*,*N*'diphenylamino)-9,9'-spirobifluorene, Spiro-DPPFPy (4).** A Young flask was charged with NaOtBu (0.079 g, 0.82 mmol), diphenylamine (0.098 g, 0.58 mmol), 2,7-bis(2,3,5,6-tetrafluoropyridin-4-yl)-2',7'-dibromo-9,9'-spirobifluorene **3** (0.200 g, 0.26 mmol) and 3.2 mL toluene. The mixture

was degassed twice and then heated up to 65º C under nitrogen atmosphere for one hour. 0.003 g of $Pd(OAc)_2$ (0.01 mmol) and 0.21 mL of a P(*tert*-Bu)$_3$ / toluene solution (0.023 g/mL, 4.8 mg, 0.02 mmol) were added via syringe and the reaction mixture was stirred at 120º C for 12 hours. The reaction mixture was cooled down to room temperature and then flash chromatographic on silica gel (DCM). The pure **4** (0.175 g, 0.18 mmol, 71 %) as a white solid was obtained by column chromatography with a mixture of *n*-hexane / EtOAc (9:1) as eluent followed by the second column chromatography with 30 % DCM in *n*-hexane as eluent. The X-ray suitable crystals were obtained by slow evaporation of solution of **4** in $CHCl_3$ / *n*-hexane (1:3) solution at ambient condition. Melting point: 293 °C (onset); glass transition temperature: 125 °C. $^1$H NMR ($CDCl_3$): δ 7.88 (d, 2H, $^3J$ = 7.8 Hz), 7.57 (d, 2H, $^3J$ = 8.2 Hz), 7.49 (m, 2H, $^3J$ = 7.8 Hz, $^4J$ = 1.5 Hz, H3, H6), 7.01 (m, 8H), 7.04 (m, 2H), 6.99 (s, 2H), 6.90 (m, 12H), 6.55 (s, 2H); $^{13}$C NMR ($CDCl_3$): δ 153.0, 150.0, 148.0, 147.5, 147.2, 144.0 (m, $^1J_F$ = 247 Hz), 142.5, 139.1 (m, $^1J_F$ = 258 Hz), 136.5, 133.4 (m), 129.6, 129.1, 128.6, 128.3, 125.8, 125.4, 124.9, 123.6, 122.6, 121.7, 121.3, 120.5, 119.9, 65.7; $^{19}$F NMR ($CDCl_3$): δ –91.1 (m, 4F), –145.6 (m, 4F); MS (APCI): *m/z* 949.35 (100, $MH^+$) HR-MS (ESI): calcd for $M^+$, 948.2494; Found: 948.2491

**X-Ray Structure analyses.** For each data collection a single crystal was mounted on a glass fibre and all geometric and intensity data were taken from this sample. X-ray crystallographic data collection using Mo-Kα radiation (λ = 0.71073 Å) was performed using a Stoe ”IPDS II” diffractometer with a Eu doped BaFCl area detector. The data sets were corrected for Lorentz and polarization effects. A numerical absorption correction by integration (X-red) was applied [S2]. The structures were solved by direct methods (SHELXS97) and refined using alternating cycles of least squares refinements against $F^2$ (SHELXL97) [S3]. All non-hydrogen atoms were found in difference Fourier maps and were refined with anisotropic displacement parameters. H atoms were placed in constrained positions according to the riding model with

the 1.2 fold isotropic displacement parameters. Graphical representations were made using ORTEP-3 win [S4].

**Electrochemical studies.**

The cyclic voltammetry measurements were performed using an EG & G Princeton 273 potentiostat/galvanostat without IR compensation. Absolute acetonitrile was used as solvent with a continuous flow of $N_2$ stream. The supporting electrolyte [*n*-$Bu_4N$][$PF_6$] (tetra-(*n*-butyl)ammonium hexafluorophosphate) (TBAHFP) was dissolved in the solvent with a concentration of 0.1 M. Pt-electrode as working electrode (diameter 4 mm), glassy-carbon electrode as counter electrode and silver/silver chloride electrode as pseudo-reference electrode were used. The scan rate was maintained at 50 mV/s. The measurements were performed versus ferrocene/ferrocenium ($Fc/Fc^+$) as internal standard reference. In-situ UV/Vis spectroelectrochemical measurements were performed using an EG & G Princeton 362 potentiostat/galvanostat with UV/Vis/NIR Lambda 9 Perkin Elmer spectrometer without IR compensation.

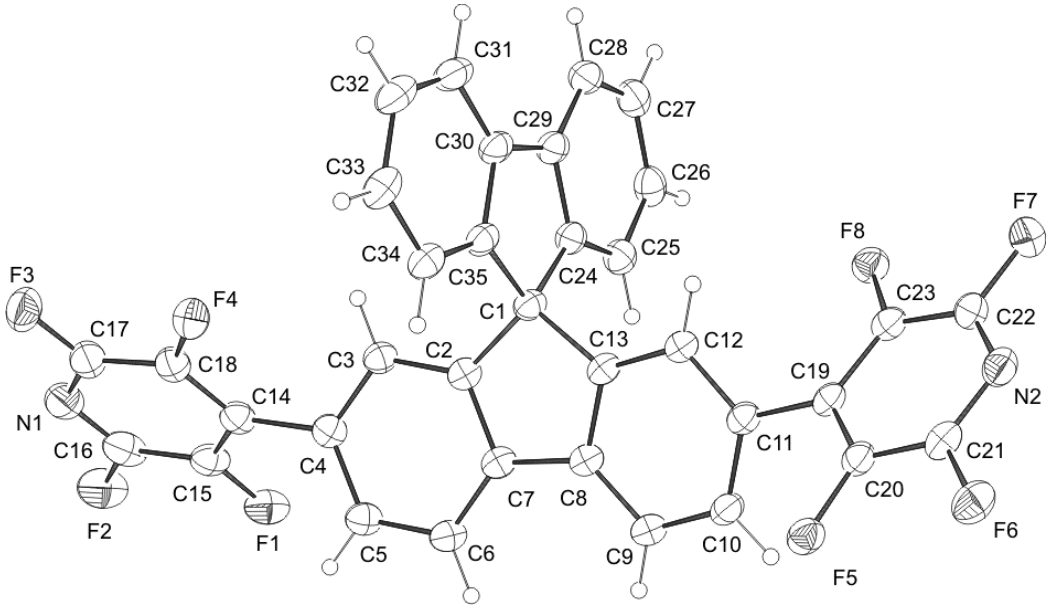


**Figure S1.** ORTEP diagram of the crystal structure of **2.** Displacement ellipsoids are drawn at 30% probability level.

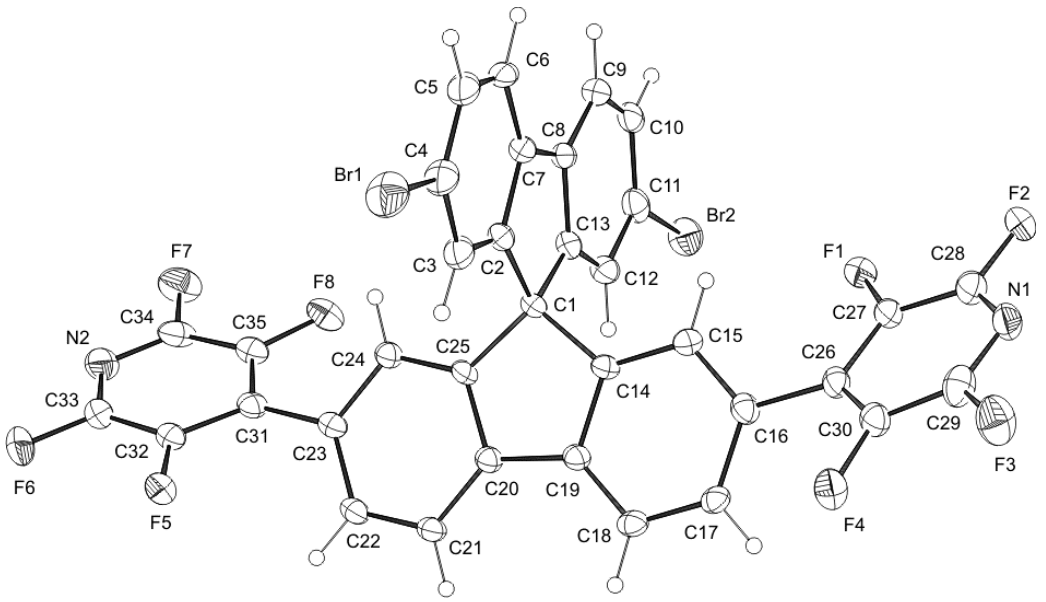


**Figure S2.** ORTEP diagram of the crystal structure of **3.** Displacement ellipsoids are drawn at 30% probability level.

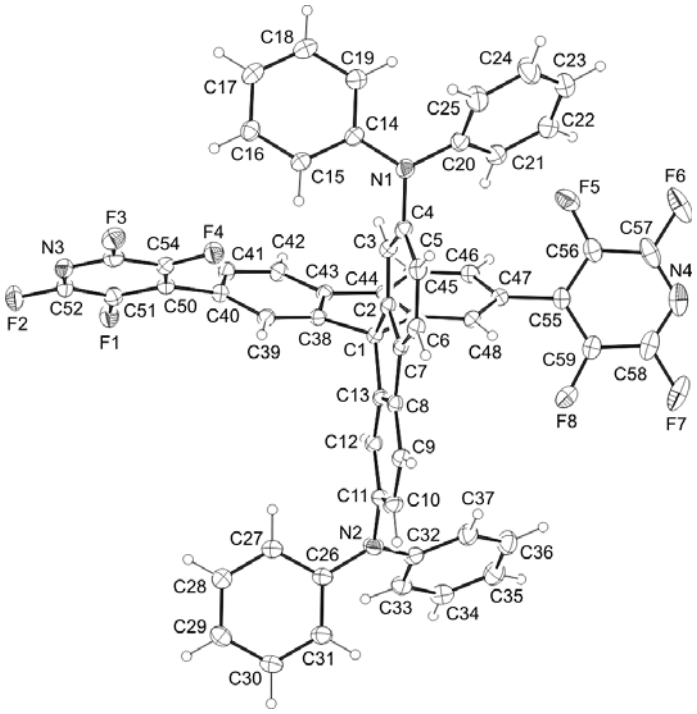


**Figure S3.** ORTEP diagram of the crystal structure of Spiro-DPPFPy **4.** Displacement ellipsoids are drawn at 30% probability level.

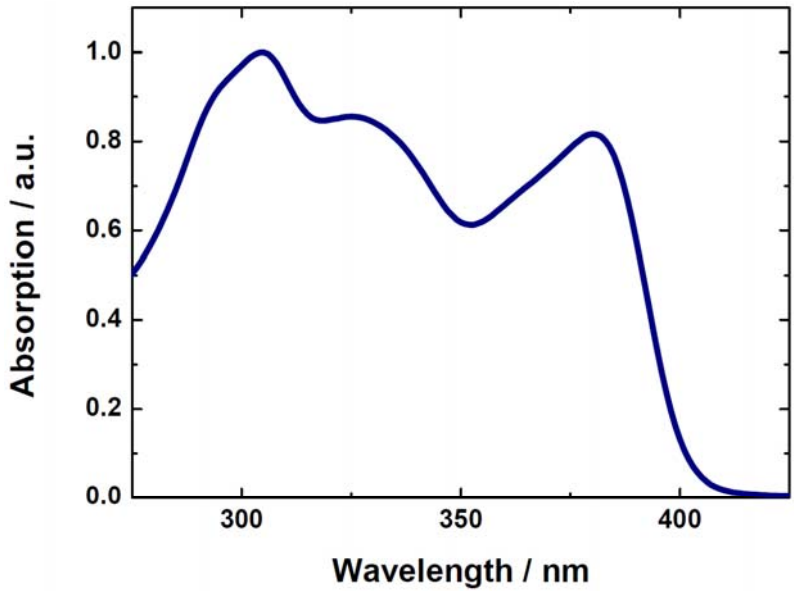


**Figure S4.** Normalized absorption spectrum of Spiro-DPPFPy **4** measured in dichloromethane. The onset of the absorption spectrum is at 400 nm (~3.1 eV).

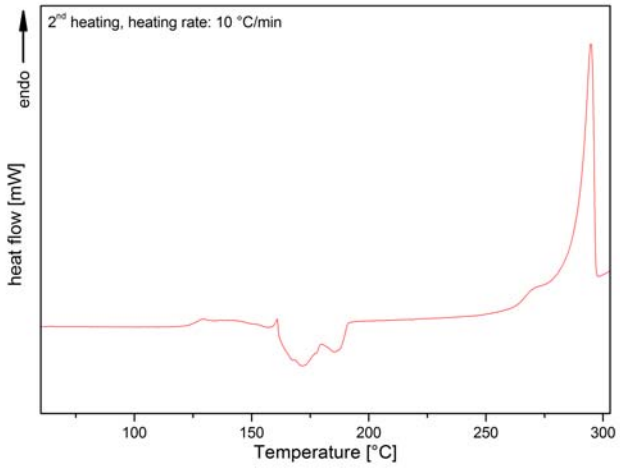


**Figure S5.** Differential scanning calorimetric curve of Spiro-DPPFPy **4**. The glass transition temperature is 125 °C. The recrystallization of the compound begins at ~ 150 °C and the material melts at ~ 293 °C (onset) with respect to the maximum peak.

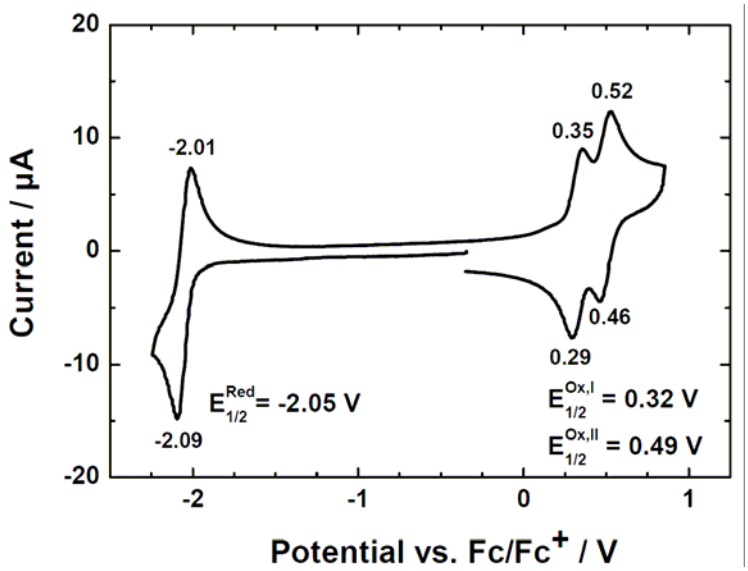


**Figure S6.** Cyclic voltammogram of Spiro-DPPFPy **4** measured in MeCN/0.1 M TBAHFP. It contains half-wave potentials of the reversible reduction and oxidation at –2.05 V ($E_{1/2}^{Red}$) +0.32 V ($E_{1/2}^{Ox,I}$) and +0.49 V ($E_{1/2}^{Ox,II}$) vs. ferrocene/ferrocenium ($Fc/Fc^{+}$), respectively. Based on the reference energy level of ferrocene of –4.8 eV, the highest occupied molecular orbital (HOMO) and lowest unoccupied molecular orbital (LUMO) levels are determined to be –5.1 eV and –2.8 eV. Thereby the equations $E_{HOMO} = -(4.8 + E_{1/2}^{Ox,I})$ and $E_{LUMO} = -(4.8 + E_{1/2}^{Red})$ are used.

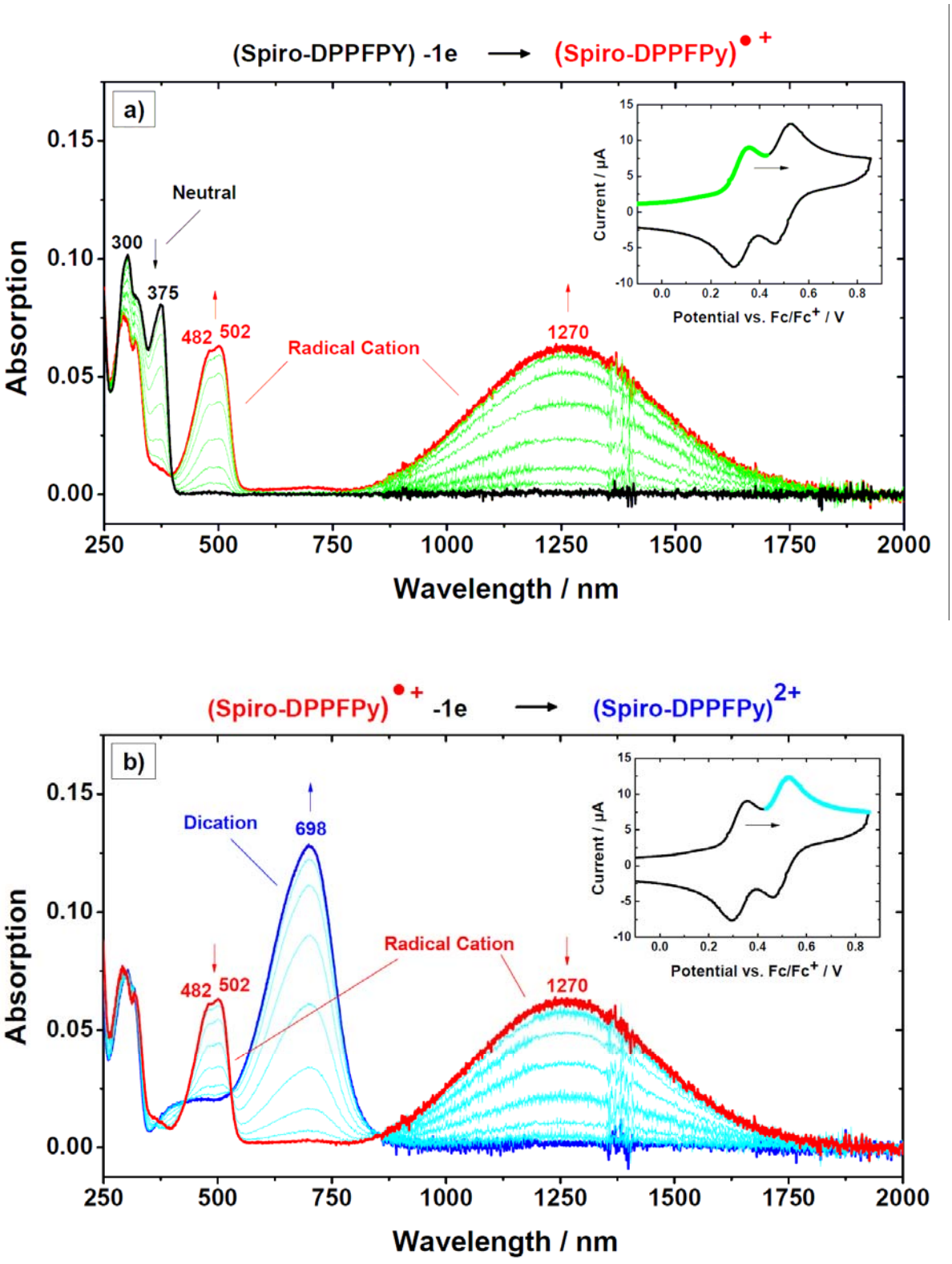


**Figure S7.** In-situ UV-Vis-NIR spectroelectrochemical measurement of Spiro-DPPFPy **4**. First (a) and second (b) oxidation in MeCN/0.1 M TBAHFP at room temperature. The inset shows the cyclic voltammogram with the corresponding potential range used in the SPEL measurement.

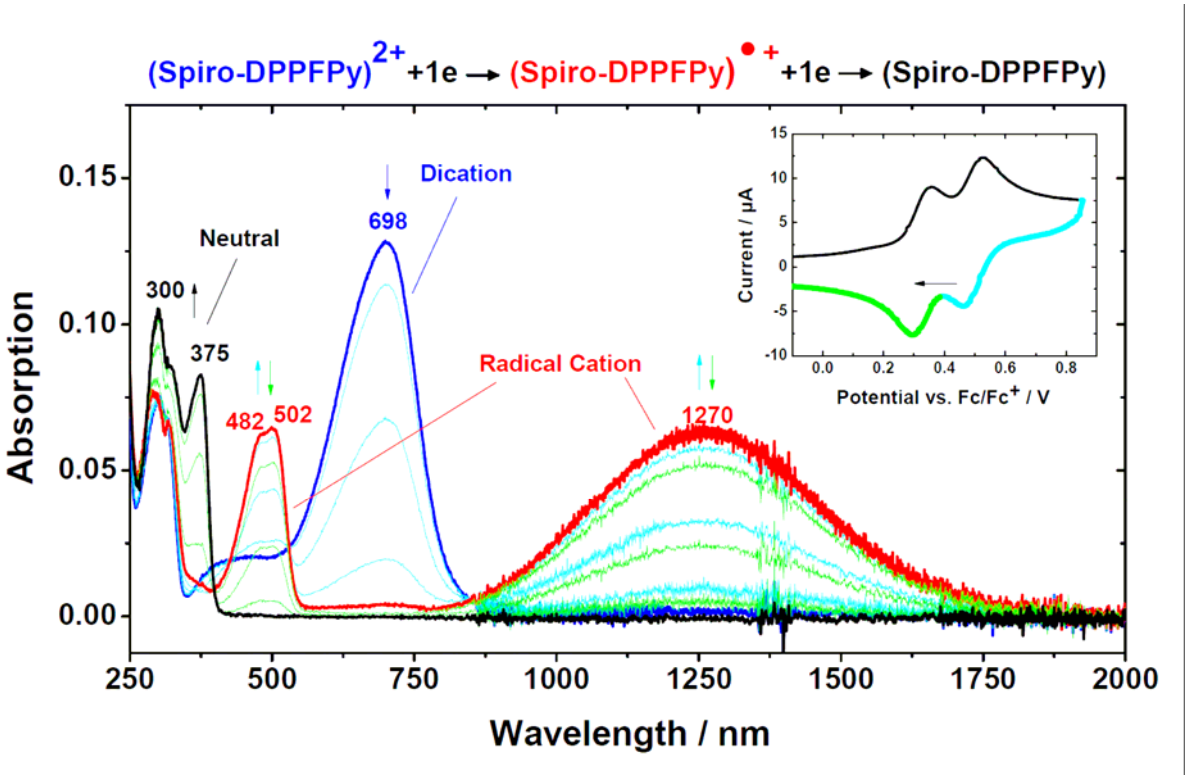


**Figure S8.** In-situ UV-Vis-NIR spectroelectrochemical measurement of Spiro-DPPFPy **4**. Reverse oxidation in MeCN/0.1 M TBAHFP at room temperature. The inset shows the cyclic voltammogram with the corresponding potential range used in the SPEL measurement.

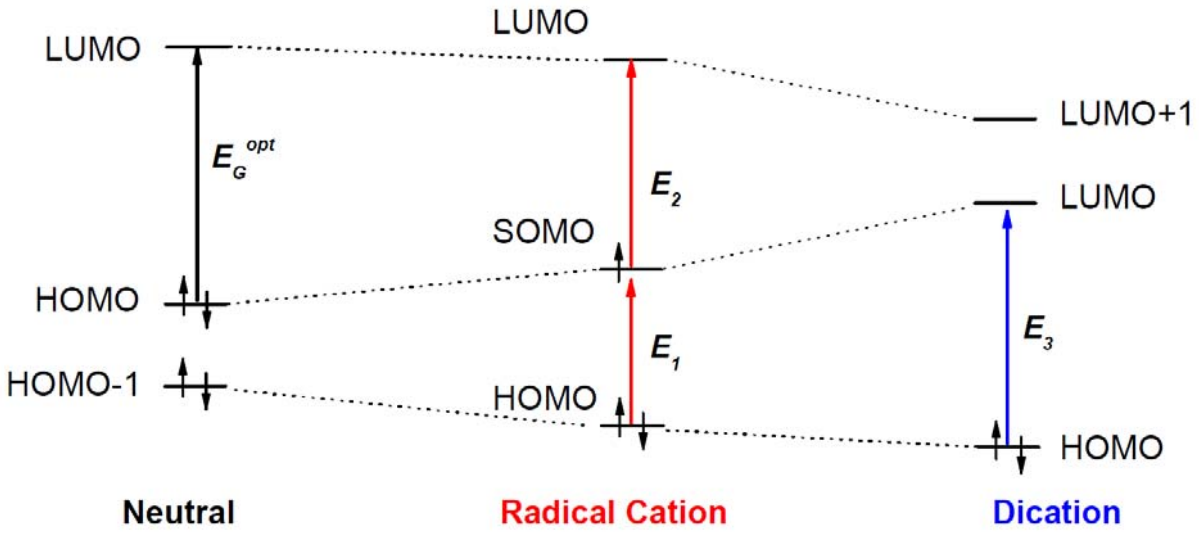


**Figure S9.** Schematic energy diagrams of the electronic structure and the optical transitions in a neutral molecule, a radical cation and a dication.

## B. Preparation and characterization of OFETs

Bottom-contact field-effect transistor substrates were purchased from Fraunhofer IPMS (Dresden, Germany) with channel lengths ($L$) between 2.5 and 20 $\mu$m and channel width ($W$) of 10 mm. The gate insulator is 230±10 nm thick $SiO_2$ and the source and drain electrodes consist of 30 nm Au with a 10 nm ITO adhesion layer. Spiro-TAD [S1], Spiro-PFPy [S5] and Spiro-DPPFPy [S5] were synthesized and purified in our laboratory. The chemical structures of these materials are depicted below:

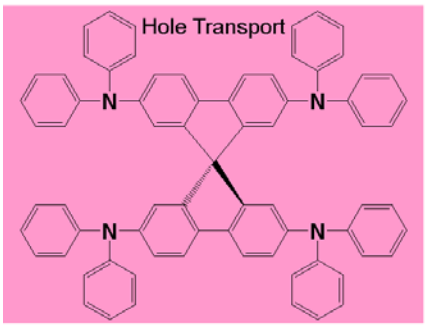


Spiro-TAD

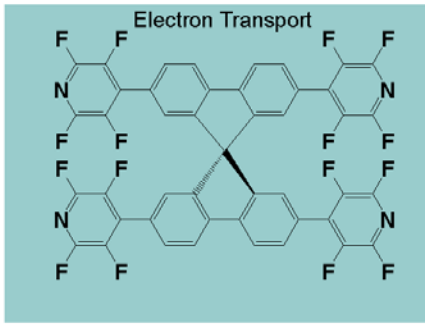


Spiro-PFPy

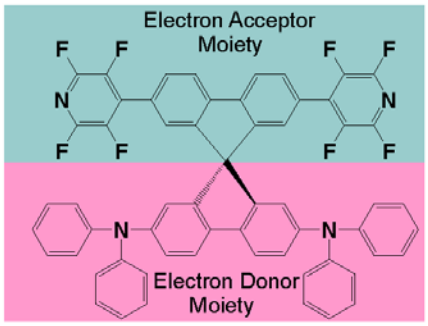


Spiro-DPPFPy

Prior to the deposition of materials, the predefined substrates were cleaned with acetone, 2-propanol and deionized water, followed by oxygen-plasma treatment and exposure to hexamethyldisilazane to replace the natural hydroxyl end-group of $SiO_2$ with an apolar methoxy group. Finally, Spiro-PFPy, Spiro-TAD and Spiro-DPPFPy were deposited by thermal evaporation at a base pressure of $1 \times 10^{-7}$ mbar ($T_{substrate}$ = 298 K) with a thickness of ~85 nm (Spiro-PFPy, Spiro-TAD, Spiro-DPPFPy devices) and 50 nm (additional

Spiro-DPPFPy devices), which was measured by spectroscopic ellipsometry. The evaporation rate was monitored by an oscillating quartz-sensor and was between 0.3 Å/s and 2.7 Å/s for all materials. From the vacuum chamber the samples were directly transferred to a glove box ($O_2$, $H_2O$ < 0.1 ppm) and placed in a homebuilt sample holder. This sample holder was placed between the poles of an (unshielded) electromagnet with the magnetic field being perpendicular to the direction of the current flow in OFETs. The magnetic field was varied between −100 mT and +100 mT. Due to the (unshielded) earth magnetic-field, reminiscence effects of the electromagnet and the uncertainty of our magnetic-field sensor, the uncertainty of our magnetic-field strength is ±80 $\mu$T. Current-voltage measurements were performed by using a Keithley 4200 semiconductor characterization system equipped with preamplifiers for improving low-current measurements. All measurements were performed inside a glove box ($O_2$, $H_2O$ < 0.1 ppm) at room temperature (≈298 K). The devices were illuminated with a Nichia NSHU 590E ultraviolet light-emitting diode ($\lambda_{max}$ = 370 nm, FWHM = 12 nm). For all measurements an illumination intensity of 132 $\mu$W was used. This intensity was measured with an AP 30UV photodetector (Scientech).

## C. Output and transfer curves of Spiro-DPPFPy OFETs

OFETs do not only offer the possibility to influence the type as well as the density of the charge carriers in the conducting channel but also to verify it. We therefore measured the output and transfer characteristics of Spiro-DPPFPy OFETs to monitor the dominant charge carrier type in our devices. No electron injection could be detected in Spiro-DPPFPy OFETs and only pure unipolar hole transport could be observed as can be seen in Fig. S10.

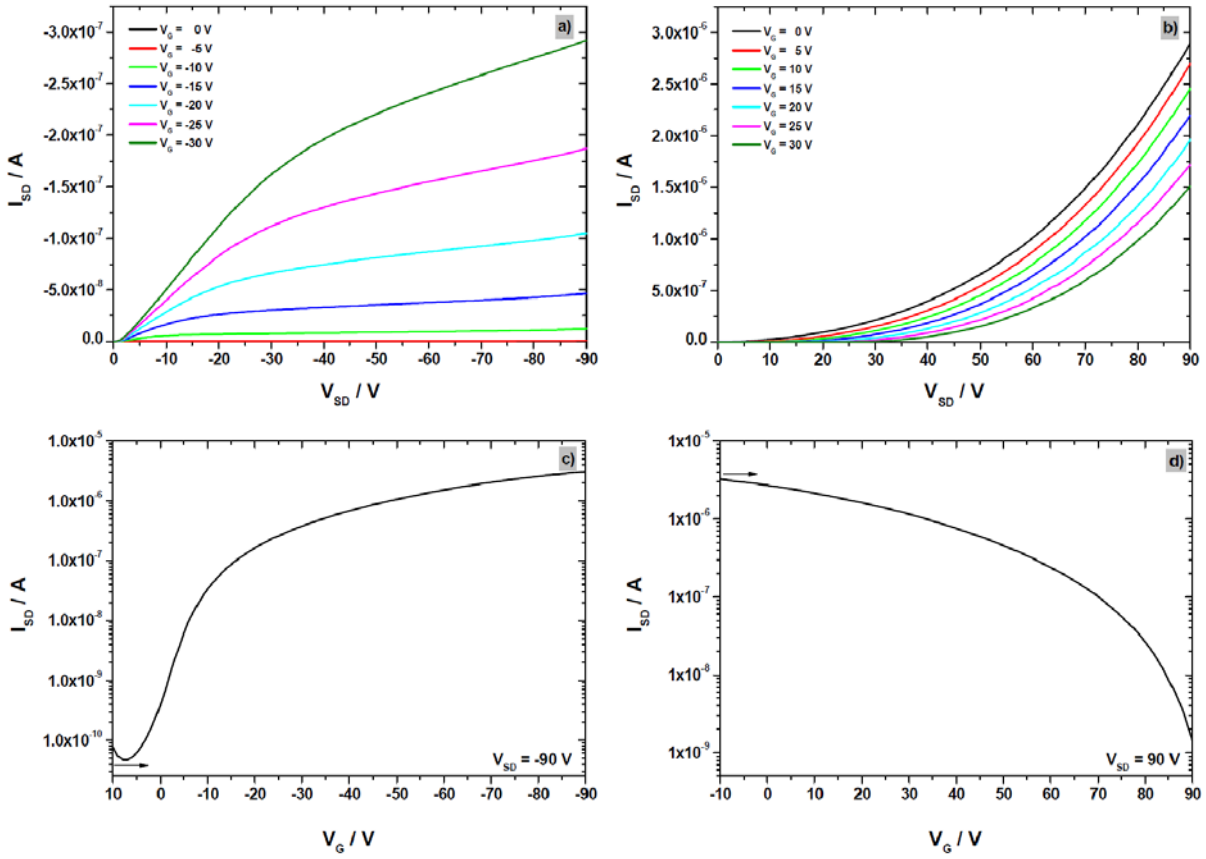


**Figure S10.** Output (a, b) and transfer (c, d) characteristics of Spiro-DPPFPy OFETs for *p*-channel (a, c) and *n*-channel (b, d). A clear gate-induced current increase is observed for *p*-channel activity, while a gate-induced current decrease can be seen in the *n*-channel. Therefore, no electrons are injected into the conducting channel of Spiro-DPPFPy for our measurement range.

We determined the field-effect hole mobility $\mu_h$ of Spiro-DPPFPy in the saturation regime ($V_{DS} = -90$ V) by using the formula $I_{DS} = (\mu_h WC/2L)(V_G - V_T)^2$ with the channel width $W$, the channel length $L$, the capacitance $C$ of the gate insulator ($SiO_2$) per unit area and the threshold voltage $V_T$. We obtained $V_T = -0.8$ V and $\mu_h = 1.4 \times 10^{-5}$ cm$^2$/Vs. The hole mobility in Spiro-TAD is $7 \times 10^{-5}$ cm$^2$/Vs [S6]. In contrast, the electron mobility in Spiro-PFPy cannot be determined due to the large energy mismatch between LUMO energy level of Spiro-PFPy and the work function of gold electrode (further discussion see text in section D and Fig. S12).

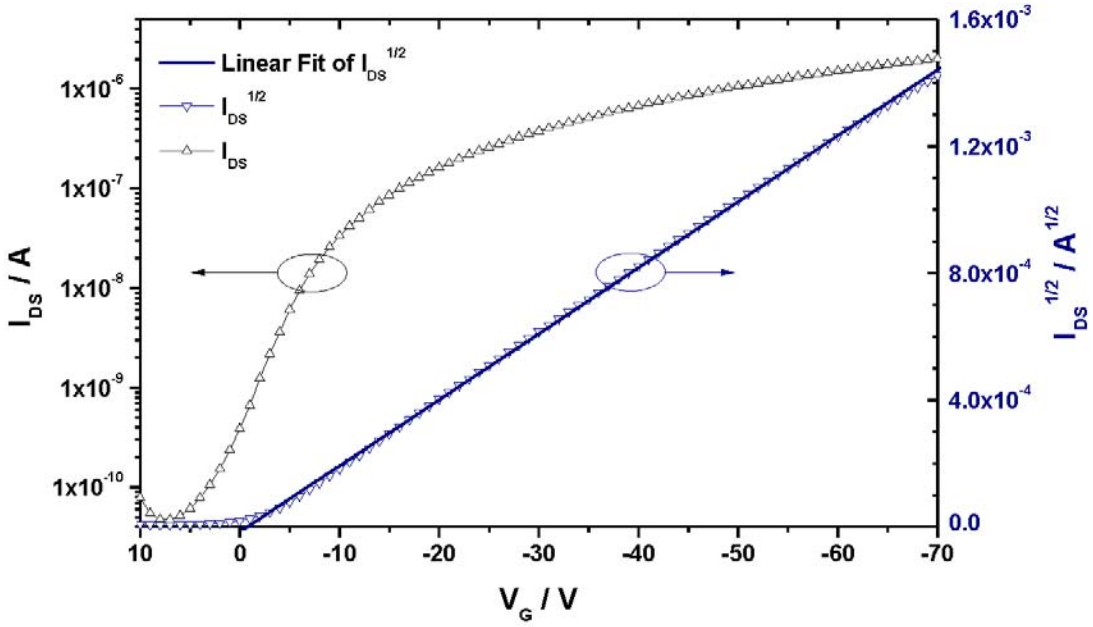


**Figure S11.** Determination of the field-effect hole mobility. $I_{DS}$-$V_G$ curve was measured at $V_{DS} = -90$ V and $I_{SD}^{1/2}$ is linearly fitted for $V_G \in [-5\text{ V}; -70\text{ V}]$.

## D. Output and transfer curves of Spiro-PFPy OFETs

The spiro-concept is based on connecting two conjugated $\pi$-systems via a common $sp^3$-hybridized carbon atom. Due to the perpendicular arrangement of the two molecular halves the interaction between the $\pi$-systems is suppressed and they preserve their basic electronic properties [S1]. While Spiro-DPPFPy consists of two different moieties, namely an electron transporting bis(perfluoropyridin-4-yl)biphenyl moiety and a hole transporting bis(diphenylamine)biphenyl moiety, Spiro-PFPy is built up of two identical bis(perfluoropyridin-4-yl)biphenyl moieties. Hence, both organic semiconductors contain the same electron transport entities.

Because of the highly decoupling properties of the spiro-concept, Spiro-DPPFPy and Spiro-PFPy are expected to have very similar electron transport properties. Therefore, measuring the output and transfer characteristics of Spiro-PFPy OFETs can be considered as an independent control experiment for the electron transport properties of Spiro-DPPFPy OFETs. As can be seen in Fig. S12 no significant source-drain current can be measured in Spiro-PFPy OFETs for all voltage conditions. The device behaves as a pure resistor in the TΩ range and the negligible source-drain current is dominated by the leakage current $I_G$ from the gate-electrode and measurement noise. All our experiments therefore clearly show that no electrons can be injected into Spiro-PFPy as well as Spiro-DPPFPy from our Au-electrodes, due to a very high injection barrier.

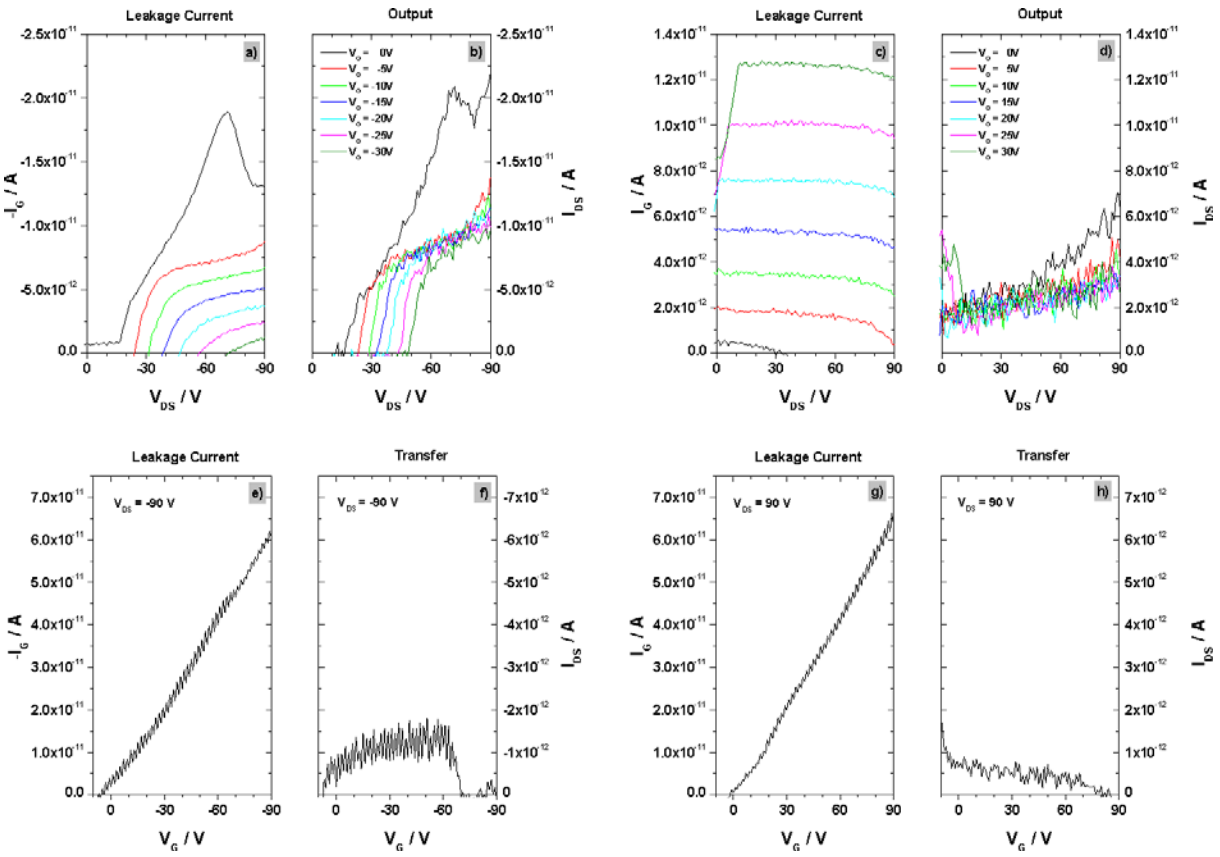


**Figure S12.** Output (b, d) and transfer (f, h) measurements as well as the corresponding leakage currents (a, c, e, g) of Spiro-PFPy OFETs for *p*-channel (a, b, e, f) and *n*-channel (c, d, g, h). The source-drain current is in the pA-range for all voltage range and is dominated by the leakage current and measurement noise. Therefore, it proves that charge (electrons or holes) injection in this case can be neglected because no significant amount of charge carriers can be injected into Spiro-PFPy.

## E. Data acquisition process and statistics

To analyse the magnetooptoelectronic properties of our devices the magnetic-field dependence of the source-drain current $I_{DS}$ was measured under constant voltage conditions with and without illumination. After baseline correction of bias stress caused drift we obtained $\Delta I_{DS}$-time curves (Fig. 1, S13, S14), where the magnetic-field induced current-change (S13) and the photoinduced current-change (S14) can clearly be seen. The determination of the corresponding magnetoresistance values and photoeffect values are described below.

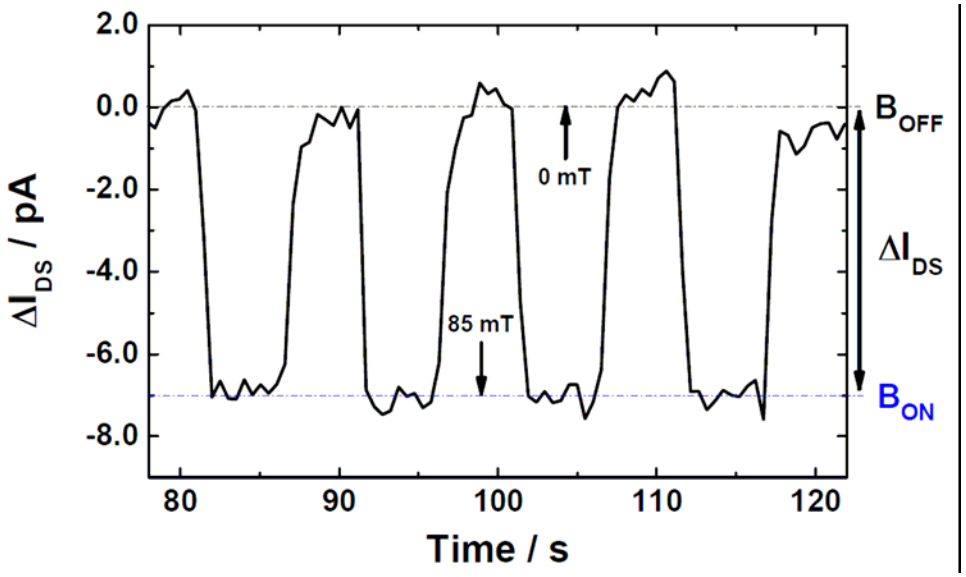


**Figure S13.** Determination of the MR values in Spiro-DPPFPy OFETs. With constant voltage conditions ($V_{DS}$ = const.; $V_G$ = const.) the magnetic-field dependency of $I_{DS}$ is analyzed. During the $I_{DS}$-measurement an external magnetic field of 85 mT is switched on and off four times in a row and $I_{DS}$-time curves like the shown one are obtained. The magnetic-field causes a current-change $\Delta I_{DS}$ which is defined as $\Delta I_{DS} = I_{DS}(B) - I_{DS}(B=0)$, where $I_{DS}(B)$ and $I_{DS}(B=0)$ are the current with and without an external magnetic-field, respectively. The MR values are calculated with $MR = \{[R(B) - R(B=0)]/R(B=0)\} \times 100\%$. R(B) and R(B=0) are resistances with and without an external magnetic-field, and are defined as $V_{DS}/I_{DS}(B)$ and $V_{DS}/I_{DS}(B=0)$. With constant $V_{DS}$ the magnetoresistance therefore is determined by $I_{DS}(B)$ and $I_{DS}(B=0)$.

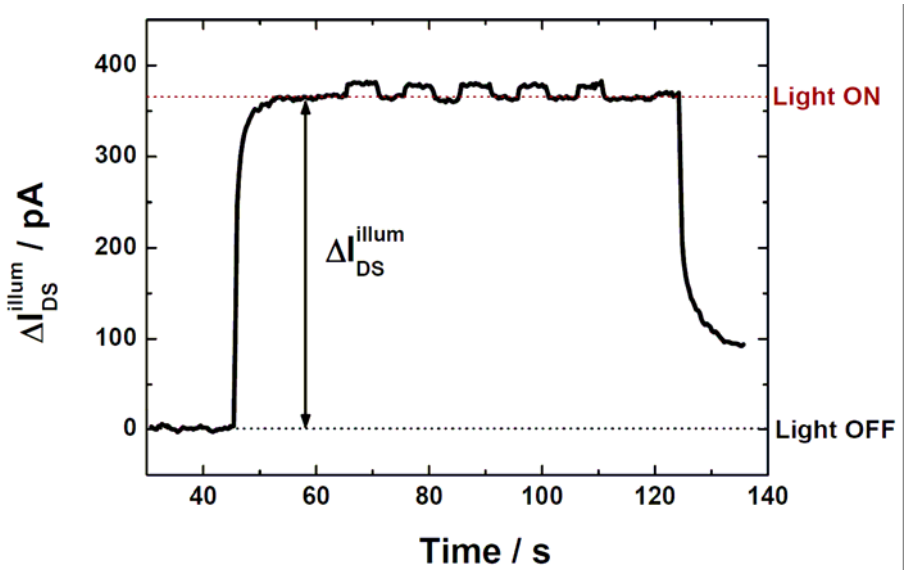


**Figure S14.** Determination of the photoeffect values in Spiro-DPPFPy OFETs. With constant voltage conditions ($V_{DS}$ = const.; $V_G$ = const.) the illumination dependency of $I_{DS}$ is analyzed. During the $I_{DS}$-measurement the Nichia NSHU 590E ultraviolet light-emitting diode ($\lambda_{max}$ = 370 nm, FWHM = 12 nm) is switched on and off and $I_{DS}$-time curves like the shown one are obtained. The illumination causes a current-change $\Delta I_{DS}^{illum}$ which is defined as $\Delta I_{DS}^{illum} = I_{DS}^{illum} - I_{DS}^{dark}$, where $I_{DS}^{illum}$ and $I_{DS}^{dark}$ are the current with and without illumination, respectively. The photoeffect (PE) values are calculated with $PE = (I_{DS}^{illum} - I_{DS}^{dark})/I_{DS}^{dark} \times 100\%$.

**Table S1.** Basic magnetoresistive behaviour of Spiro-DPPFPy OFETs with variable channel lengths, film thickness and evaporation rates.

| Sample number | Channel length[a] / µm | Film thickness / nm | Evaporation rate / Å$s^{-1}$ | Sign of MR in darkness[b] | Sign of MR under illumination[c] |
|---|---|---|---|---|---|
| 837_Tr. 1 | 2.5 µm | 85 | 2.7 | + | – |
| 837_Tr. 2 | 2.5 µm | 85 | 2.7 | + | – |
| 837_Tr. 3 | 2.5 µm | 85 | 2.7 | Defect | |
| 837_Tr. 4 | 2.5 µm | 85 | 2.7 | + | – |
| | | | | | |
| 872_Tr. 1 | 2.5 µm | 50 | 0.3 | n.d. | – |
| 872_Tr. 2 | 2.5 µm | 50 | 0.3 | + | – |
| 872_Tr. 3 | 2.5 µm | 50 | 0.3 | + | – |
| 872_Tr. 4 | 2.5 µm | 50 | 0.3 | n.d. | – |
| | | | | | |
| 872_Tr. 1 | 5 µm | 50 | 0.3 | + | – |
| 872_Tr. 2 | 5 µm | 50 | 0.3 | n.d. | – |
| 872_Tr. 3 | 5 µm | 50 | 0.3 | + | – |
| 872_Tr. 4 | 5 µm | 50 | 0.3 | n.d. | – |
| | | | | | |
| 872_Tr. 1 | 10 µm | 50 | 0.3 | Defect | |
| 872_Tr. 2 | 10 µm | 50 | 0.3 | n.d. | – |
| 872_Tr. 3 | 10 µm | 50 | 0.3 | + | – |
| 872_Tr. 4 | 10 µm | 50 | 0.3 | + | – |
| | | | | | |
| 872_Tr. 1 | 20 µm | 50 | 0.3 | + | – |
| 872_Tr. 2 | 20 µm | 50 | 0.3 | + | – |
| 872_Tr. 3 | 20 µm | 50 | 0.3 | n.d. | – |
| 872_Tr. 4 | 20 µm | 50 | 0.3 | + | – |

[a]: The channel width is 10 mm for all devices.
[b]: B = 60 mT.
[c]: B = 60 mT, illumination intensity of 132 $\mu$W ($\lambda_{max}$ = 370 nm).
n.d.: MR value cannot be determined because the change in current due to magnetic field is comparable to the measurement noise.

## F. Magnetoresistance of illuminated devices

We determined the magnetoresistance of illuminated Spiro-DPPFPy OFETs over a wide range of gate-voltages. MR values as high as −6.5% can be obtained near the switch-on voltage.

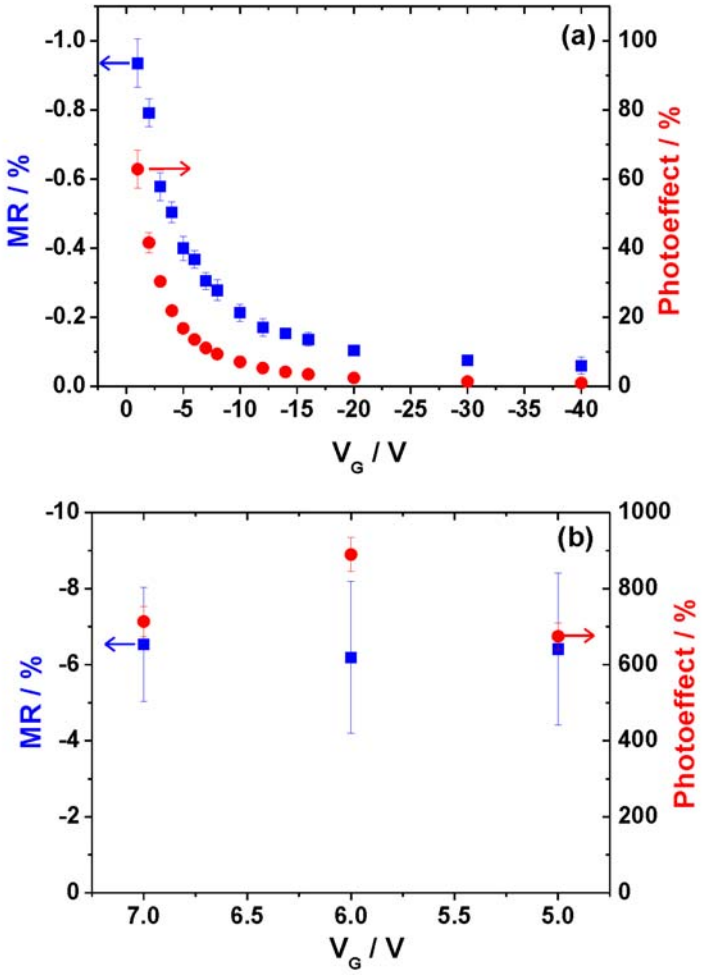


**Figure S15.** Magnetoresistance in illuminated Spiro-DPPFPy OFETs for the on-state (a) and the off-state (b). The measurements were performed with $V_{DS}$ = −5 V and B = 85 mT.

## F. Magnetic Field Dependence

We also measured the magnetoresistance values at different magnetic field strengths. However, it was difficult to obtain magnetoresistance values in darkness measured at different magnetic field strengths due to three reasons: (i) the magnetoresistance value is really small (~0.1% at 85 mT), (ii) our measurement set-up is limited by the magnetic field strength itself (~100 mT), and (iii) relative low ratio of signal to noise for measurements at low magnetic fields. Fortunately, we could measure magnetoresistance values at different magnetic field strengths upon illumination, as shown in Fig. S16. In this case the non-Lorentzian line shape (MR = a $B^2/(|B|+B_0)^2$) fitted our data better than the Lorentzian line shape (MR = a $B^2/(B^2+B_0^2)$), whereas MR is the magnetoresistance in percent, a is a fitting parameter, B is the magnetic field and $B_0$ is the half-saturation field.

| | **Non-Lorentzian line shape** | **Lorentzian line shape** |
|---|---|---|
| **R (correlation-coefficient)** | 0.99857 | 0.9922 |
| **a** | (-1.59±0.03) % | (-1.24±0.04) % |
| **$B_0$** | (11.1±0.5) mT | (18.4±1.3) mT |

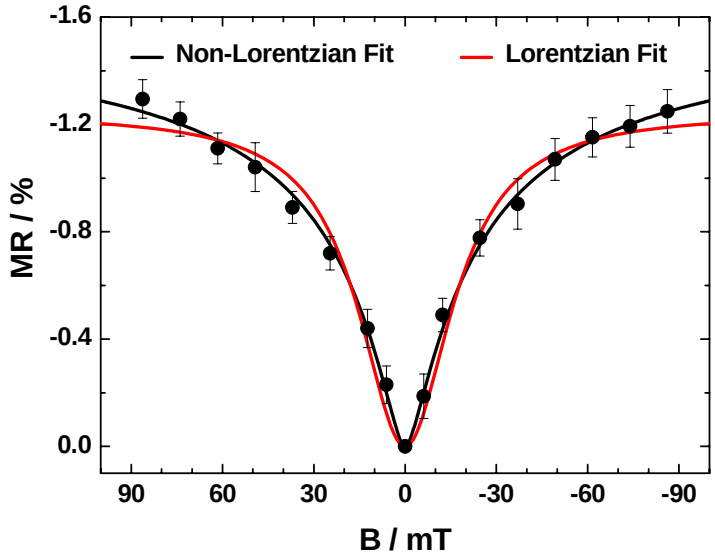


**Figure S16.** Magnetic field dependence measurement of field-effect transistor upon illumination condition (illumination intensity of 132 $\mu$W, $\lambda_{max}$ = 370 nm). The measurements were performed at $V_{DS}$ = –5 V and $V_G$ = –1 V.

[S1] T. P. I. Saragi, T. Spehr, A. Siebert, T. Fuhrmann-Lieker and J. Salbeck, *Chem. Rev.* 2007, **107**, 1011.

[S2] Stoe & Cie GmbH; X-red ver. 1.31, Program for numerical absorption correction, Darmstadt, Germany, 2004.

[S3] G. M. Sheldrick, SHELXS 97 and SHELXL 97, Programs for crystal structure solution and refinement, University of Göttingen, Germany, 1997.

[S4] L. J. Farrugia, J. *Appl. Crystallogr.* 1999, **32**, 837.

[S5] E. Tatarov, PhD Thesis, University of Kassel, Germany, 2011.

[S6] T. P. I. Saragi, T. Fuhrmann-Lieker and J. Salbeck. *Synth. Met.* 2005, **148**, 267.